Research Square

Preprints are preliminary reports that have not undergone peer review.
They should not be considered conclusive, used to inform clinical practice,
or referenced by the media as validated information.

Effects of Chamber Geometry on Hydrodynamic Response and Pneumatic Power Conversion in L-Shaped Oscillating Water Column Devices

Esti Ratnasari
National Research and Innovation Agency
Ayu Novitasari Saputri
National Research and Innovation Agency
Endarto Tri Wibowo
National Research and Innovation Agency
Wahyu Hendriyono
wahyu.hendriyono@brin.go.id

National Research and Innovation Agency
Andan Sigit Purwoko
National Research and Innovation Agency
Agus Wibowo
National Research and Innovation Agency
Johan Risandi
National Research and Innovation Agency
Ahmad Taufiqur Rohman
National Research and Innovation Agency
Dinar Catur Istiyanto
National Research and Innovation Agency
Adnan Sandy Dwi Marta
National Research and Innovation Agency

Research Article

Keywords: Oscillating Water Column, chamber geometry, hydrodynamic–pneumatic coupling, near-resonant waves, wave energy conversion, experimental modelling

Posted Date: July 2nd, 2026

DOI: https://doi.org/10.21203/rs.3.rs-10178607/v1

License: This work is licensed under a Creative Commons Attribution 4.0 International License.
Read Full License

Additional Declarations: No competing interests reported.

Effects of Chamber Geometry on Hydrodynamic Response and Pneumatic Power Conversion in L-Shaped Oscillating Water Column Devices

Esti Ratnasari[1], Ayu Novitasari Saputri[1], Endarto Tri Wibowo[1], Wahyu Hendriyono[1], Andan Sigit Purwoko[1], Agus Wibowo[2], Johan Risandi[3], Ahmad Taufiqur Rohman[4], Dinar Catur Istiyanto[1], Adnan Sandy Dwi Marta[1,2]

Corresponding authors: W. Hendriyono (wahyu.hendriyono@brin.go.id), A. S. D. Marta (adna001@brin.go.id)

1) Research Centre for Hydrodynamics Technology, National Research and Innovation Agency (BRIN), Yogyakarta, Indonesia
2) Directorate for Laboratory Facilities, and Science and Technology Park, National Research and Innovation Agency (BRIN), Yogyakarta, Indonesia
3) Research Centre for Oceanology, National Research and Innovation Agency (BRIN), Jakarta, Indonesia
4) Research Centre for Conversion Energy Technology, National Research and Innovation Agency (BRIN), Tangerang, Indonesia

Abstract

This study presents an experimental investigation of the hydrodynamic–pneumatic performance of three L-shaped Oscillating Water Column (OWC) chamber geometries subjected to near-resonant regular wave conditions. Laboratory experiments were conducted in a wave flume using a 1:10 scale model to evaluate the influence of chamber geometry on free-surface elevation, air-pressure oscillations, airflow velocity, pneumatic power output, and overall energy conversion efficiency. Measurements were obtained under controlled wave forcing (H = 0.225 m) across a range of wave periods representative of resonance conditions. The results demonstrate that chamber geometry strongly governs the coupled hydrodynamic–pneumatic response. Geometry 2 achieved the most stable piston-type water-column motion, coherent pressure fluctuations, and consistent airflow, resulting in the highest pneumatic efficiency and power performance. In contrast, Geometry 1 exhibited strong hydrodynamic excitation but significant internal flow irregularities that reduced conversion efficiency, while Geometry 3 generated large oscillation amplitudes accompanied by nonlinear instability and energy dissipation. The findings show that large oscillation amplitudes alone do not guarantee improved energy extraction; rather, stability and phase coherence between hydrodynamic and pneumatic processes are critical for efficient operation. This study provides experimentally validated insights into geometry-dependent resonance behaviour and establishes a multi-parameter framework for optimising OWC chamber design toward more stable and efficient wave energy converters.

Keywords: Oscillating Water Column; chamber geometry; hydrodynamic–pneumatic coupling; near-resonant waves; wave energy conversion; experimental modelling.

1. Introduction

The growing urgency to reduce dependence on fossil fuels has intensified global efforts to develop renewable energy sources capable of mitigating climate change while ensuring long-term energy security. Among the available options, wave energy is particularly attractive due to its high energy density and relatively stable availability when compared with solar and wind resources (Gadelho et al., 2024). Given that oceans cover more than two-thirds of the Earth's surface, wave energy represents a vast and geographically widespread resource with considerable potential for large-scale power generation. In response, a wide range of wave energy converter (WEC) technologies has been developed in recent decades to harness this abundant renewable resource (Rezanejad et al., 2019). A fundamental challenge associated with WEC deployment lies in their ability to operate efficiently under highly variable wave conditions. Ocean waves exhibit substantial variability in height, period, and duration, requiring conversion systems to perform reliably across a broad spectrum of wave climates. Among the various WEC concepts, the OWC has emerged as one of the most promising technologies due to its relatively simple structure, robustness, and proven potential for efficient wave energy conversion (Juan et al., 2022). WECs such as oscillating water columns or point absorbers are commonly tailored to local depth and wave period characteristics (Hendriyono et al., 2026). WECs are generally designed according to site-specific hydrodynamic conditions to maximise energy extraction efficiency. Most OWC devices consist of a semi-submerged chamber that traps a water column, coupled with an air turbine connected through an orifice. Incident waves induce oscillatory motion of the internal water column, causing the enclosed air to be alternately compressed and decompressed. This bidirectional airflow passes through the turbine, enabling the conversion of wave-induced hydrodynamic energy into electrical power (Ning et al., 2024). The efficiency of this initial hydrodynamic-to-pneumatic conversion stage is of critical importance, as it is widely recognized that insufficient performance at

this step remains a primary barrier to the large-scale commercialization of OWC technology (Çelik & Altunkaynak, 2020; Hsieh et al., 2012; Mandev et al., 2024).

Accordingly, recent research on OWC systems has increasingly focused on the role of geometric optimization in enhancing energy conversion performance. Experimental and numerical studies have shown that key geometric parameters (including chamber width, wall thickness, bottom slope, and orifice size) exert a strong influence on hydrodynamic response and pneumatic efficiency. (Ning et al., 2017) investigated a land-based single-chamber OWC incorporating an internal submerged barrier, where airflow generated by dual oscillatory motions drives a single power take-off (PTO) system. Their quantitative analysis demonstrated that the introduction of dual sub-chambers can significantly improve hydrodynamic performance, particularly under short-wave conditions. Subsequently, (Ning et al., 2019) examined the hydrodynamic behavior of a land-based dual-chamber OWC integrated with a coastal structure, revealing that a small skirt draft can substantially enhance energy conversion and that the rear chamber consistently extracts more hydrodynamic power than the front chamber. It has found that a tiny skirt draft can contribute to boosting the hydrodynamic energy conversion, and the rear chamber extracts more hydrodynamic power than the front chamber. Complementary to these findings, (R. quan Wang et al., 2020) analyzed wave loads acting on the front and central walls of a land-based dual-chamber OWC for various geometric configurations, including sub-chamber width and skirt-wall dimensions, highlighting the strong dependence of structural loading and hydrodynamic performance on geometric design choices.

Furthermore, (EL Bouji et al., 2023) reported that variations in these parameters significantly altered airflow velocity and power output, indicating the necessity of geometric optimization for maximizing device efficiency. Their findings further highlighted that the coupling between chamber geometry and installation conditions could yield considerable improvements in hydrodynamic performance. (Zhao et al., 2021) experimentally evaluated the hydrodynamic energy conversion performance of single-, dual-, and triple-chamber OWC systems by examining the wave dissipation coefficient. Their findings indicated that the triple-chamber configuration achieved superior energy extraction efficiency compared to the single- and dual-chamber devices.

Meanwhile, (J.-S. Kim & Nam, 2022) conducted numerical investigations of the energy conversion characteristics of OWC devices with one, two, and three chambers using time-domain simulations grounded in potential theory. It has been provided detailed insights into the hydrodynamic behavior of the internal fluid within the OWC chamber, including sloshing motions and piston-type oscillations. Hydrodynamic behavior inside the OWC chamber encompassing phenomena such as sloshing and piston-type oscillations has been a central focus of recent investigations. Based on research (Zheng et al., 2020) conducted numerical analyses on the hydrodynamic performance of multi-chamber OWC systems ranging from single- to quintuple-chamber configurations, emphasizing the influence of geometrical parameters including chamber width, wall thickness, and draft.

To further enhance hydrodynamic efficiency, (R. quan Wang et al., 2020) proposed an innovative dual-chamber OWC design featuring pitching front walls, introducing a new mechanism aimed at improving wave–structure interaction and energy conversion. Moreover, (C. Wang et al., 2022) developed a novel dual-chamber OWC device featuring dual pitching lip-walls located at the front and mid positions to enhance energy extraction across a broader range of wave frequencies. Using a semi-analytical model based on potential-flow theory, the study demonstrated that coordinated pitching motions significantly improve hydrodynamic performance compared to stationary or single-pitching configurations. The results revealed that optimal combinations of lip-wall drafts and angle-spring stiffness can markedly increase power absorption, while the dual-pitching design enables more effective utilization of both chambers, particularly under short-period wave conditions. (J. S. Kim et al., 2023) experimentally confirmed that multi-chamber OWC configurations outperform single-chamber systems. Their results showed that dividing the chamber into multiple sections reduces sloshing effects, increases pneumatic power production, and smooths power fluctuations. The study also reported that asymmetric triple-chamber geometries can further enhance energy capture by improving wave-trapping efficiency.

In addition, numerical and experimental investigations have examined modified chamber designs, such as projecting-wall and L-shaped OWC systems. (Tan et al., 2024) conducted computational fluid dynamics (CFD) simulations of a projecting-wall OWC, showing that wall geometry affected phase differences between internal water oscillations and chamber air pressure, which in turn influenced energy absorption. Their results indicated that careful geometric modifications could enhance the capture width ratio and improve overall device stability. Correspondingly, (Mocellin et al., 2024) evaluated a variety of geometric configurations using regular sea states and confirmed that geometry strongly influences internal air-flow dynamics and pneumatic conversion.

Further investigations reinforce the critical influence of chamber geometry on hydrodynamic–pneumatic coupling. (Rezanejad et al., 2021) showed that geometric modifications to the front-wall and opening submergence significantly alter wave–structure interaction, internal resonance behavior, and the phase relationship between free-surface motion and air-pressure fluctuations. Their results indicate that appropriate geometric tuning can enhance energy extraction by improving pressure buildup and stabilizing the pneumatic response. Likewise, (Elhanafi et al., 2018) showed through coupled CFD–FEM modeling that variations in

chamber length, opening submergence, and front-wall inclination can suppress sloshing instabilities and significantly strengthen pneumatic pressure peaks

Despite these advances, much of the existing research has concentrated on isolated performance indicators, such as energy conversion efficiency or chamber resonance, often neglecting the complex interactions among multiple parameters. As a result, the broader relationships between geometry, internal dynamics, and efficiency remain insufficiently explored. This research gap underscores the need for comprehensive multi-parameter analyses of L-shaped OWCs to better understand how geometric configurations collectively affect performance under varying wave conditions.

The performance of L-shaped OWC devices is highly dependent on their geometric configuration, including parameters such as chamber length-to-width ratio, duct orientation, and immersion depth. Prior studies have demonstrated that geometric modifications, such as altering the front wall into an L-shape or adjusting chamber dimensions, can significantly influence energy conversion efficiency (Nguyen et al., 2024; Samak et al., 2021). Similarly, experimental and numerical investigations have shown that variations in wall thickness, chamber slope, or entrance duct length affect not only the pneumatic efficiency but also the internal hydrodynamics of the system (de Lima et al., 2024; EL Bouji et al., 2023).

Despite these advances, most studies tend to focus on a limited set of performance parameters, such as power efficiency or capture width ratio, while overlooking the complex internal dynamics that govern system behavior. For example, (Samak et al., 2021) highlighted that changes in entrance duct length of an L-OWC affected air pressure and free-surface motion, yet the analysis remained confined to specific performance outputs. Likewise, (Lin et al., 2023) applied artificial neural networks for geometry optimization, but the focus was primarily on maximizing capture factor, without a comprehensive multi-parameter evaluation. This gap highlights the need for research that simultaneously considers multiple interdependent performance indicators. In particular, understanding how geometric variations affect internal parameters such as chamber air pressure, FSE, and fluid velocity, is crucial for identifying optimal designs. A systematic multi-parameter analysis would therefore provide a more holistic basis for the design and optimization of L-OWC devices, ensuring not only higher energy output but also improved stability and operational efficiency.

The primary objective of this research is to optimize the design of L-OWC devices through a comprehensive multi-parameter analysis of diverse geometric configurations. In contrast to earlier works that have largely concentrated on energy conversion efficiency as the principal indicator of performance, this study extends the scope of investigation to a broader set of interdependent hydrodynamic and pneumatic variables. The analysis is directed toward understanding how modifications in chamber geometry influence internal air-pressure dynamics, the oscillatory behavior of the free surface, and the resulting pneumatic power output. In addition, the study incorporates the evaluation of non-dimensional performance parameters, such as capture width ratio and phase relationships between pressure and velocity, to establish a scalable framework for design optimisation.

It should be emphasized that the L-shaped chamber investigated in this study is not a novel concept, but rather a continuation of previous experimental developments conducted in our laboratory, where the baseline L-chamber configuration was initially established and validated. Building upon this foundation, the present study focuses on optimizing key internal geometric parameters, particularly the horizontal chamber length and internal flow path characteristics, to better understand their influence on hydrodynamic stability and pneumatic power generation. The selection of the L-shaped Oscillating Water Column (L-OWC) is supported by its demonstrated hydrodynamic advantages over conventional configurations, such as U-shaped and vertical chambers (Supriyanto et al., 2025). The incorporation of a horizontal duct aligned with wave propagation enhances resonance characteristics while reducing wave radiation damping, thereby improving system efficiency (Putri et al., 2026). Previous experimental studies have further shown that this configuration can generate larger free surface oscillations (serving as the primary driver of pneumatic power conversion) and achieve higher wave amplification, with Wave Amplification Factor (WAF) values reaching up to 3.21 at specific depth-to-wavelength (d/L) ratios (Supriyanto et al., 2025; Putri et al., 2026). These findings highlight the strong potential of the L-OWC configuration for enhanced energy capture, particularly under short-period wave conditions.

The effectiveness of the L-OWC is further evidenced by its high pneumatic power conversion performance, where the system can achieve a peak power efficiency of up to 98.2% under specific wave height and period variations (Marta et al., 2024). A crucial technical characteristic of this design is the dominance of the decompression phase, where airflow velocities are consistently higher than during the compression phase, providing optimal opportunities for the use of more efficient radial turbines or unidirectional systems (Malakani et al., 2026; Putri et al., 2026). The validity of the L-shaped design is not limited to laboratory scales but has been proven through full-scale implementation by Wave Swell Energy (WSE) in the UniWave200 project at King Island, Australia, which reported an energy conversion efficiency of 48% in real sea conditions (Marta et al., 2024). Thus, the choice of L-shaped geometry is a highly rational decision supported by robust empirical data in maximizing differential pressure and airflow velocity for optimal wave energy conversion (Marta et al., 2024; Supriyanto et al., 2025). In contrast to prior studies that predominantly examine isolated performance indicators or emphasise single-parameter geometric optimisation, the present work introduces a comprehensive experimental

framework that simultaneously evaluates free-surface elevation, internal air-pressure dynamics, air-velocity coherence, pneumatic power generation, and overall conversion efficiency across multiple L-OWC geometries. This integrated approach provides the first systematic characterisation of how geometry-driven variations govern the coupled hydrodynamic–pneumatic response under near-resonant wave forcing an operational regime where nonlinear interactions and measurement instabilities are most pronounced. By directly linking geometric configurations to the full chain of internal dynamic processes, this study uncovers previously overlooked interdependencies that fundamentally shape device performance. The resulting insights offer a novel foundation for geometry-informed optimisation strategies and contribute to the development of more stable and higher-efficiency next-generation OWC systems.

The remainder of this paper is structured as follows. The next section describes the experimental methodology employed in this study, including the design of the experimental modelling setup, the tested geometric configurations, and the procedures for data collection. This is followed by a presentation of the experimental results and a discussion of the key findings, with particular emphasis on how geometric variations influence the hydrodynamic and pneumatic performance of the L-OWC. Finally, the paper concludes by summarising the main outcomes and outlining of practical implications for the future design and optimisation of wave energy conversion systems.

It should be noted that the present study is conducted under regular wave conditions, which provide a controlled framework to isolate the fundamental hydrodynamic and pneumatic behavior of the OWC system. This approach is particularly useful for identifying resonance characteristics and phase interactions between the oscillating water column and the air chamber. The relative performance trends between chamber geometries observed in this study are expected to remain qualitatively valid. This is because the dominant governing mechanisms namely resonance behavior and air compressibility effects continue to play a key role under irregular wave excitation, although their magnitude and optimal operating conditions may vary.

2. Materials and methods

The present study adopts a laboratory-scale experimental approach to analyse the influence of OWC chamber geometry on hydrodynamic characteristics and wave energy conversion efficiency. Three geometric configurations, including geometry 1 (Geo 1), geometry 2 (Geo 2), and geometry 3 (Geo 3) were tested under regular wave conditions with a controlled wave height of $H = 0.225$ m.

2.1 Experimental modelling setup

The laboratory experiments were conducted in a rectilinear wave flume with internal dimensions of 1.0 m in width, 1.5 m in depth, and 36.0 m in length. A piston-type wavemaker equipped with active stroke control generated regular incident waves of specified amplitude and period. The flume configuration adhered to IAHR physical modelling requirements to ensure adequate fetch, minimal wall-induced interference, and normal wave incidence on the model. These considerations were essential for preserving Froude similarity and ensuring that the hydrodynamic field developed without directional distortion (HYDRALAB III, 2011).

The model OWC device was positioned 7 m upstream of the dissipative wave absorber to suppress first- and higher-order reflections, and 3 m downstream of the wavemaker to allow full establishment of the wave kinematics before reaching the measurement zone. The prescribed wave conditions were selected within the validity range of linear Airy theory, corresponding to prototype-equivalent periods of 6.5–14.5 s and incident wave heights up to 2.25 m. The geometric configuration of the flume and chamber ensured that the internal resonance, free-surface oscillations, and hydrodynamic loading could be measured under controlled and repeatable conditions.

2.2 The OWC scaled model

The physical model was constructed at a geometric scale of 1:10 based on the Froude similarity law, ensuring that gravity-dominated hydrodynamic processes observed in the laboratory reproduced the corresponding prototype behaviour. This scaling approach preserves the correct ratio between inertial and gravitational forces, allowing chamber resonance, pressure oscillations, and water-column kinematics to be meaningfully extrapolated to full scale.

The experimental setup employed a L-OWC device consisting of a vertical inlet column, a horizontal air–water interaction duct, and an upper chamber section intended to house a turbine. Key structural dimensions include a vertical water-column height of approximately 1.44 m, an immersion depth of 1.20 m under still-water conditions, and a horizontal duct length ranging from 0.505 m to 0.905 m depending on the configuration tested that it can be seen in Fig.1 and Fig.2. The chamber incorporates a converging–diverging internal geometry with

30° inclined walls guiding the flow toward a throat region. This contouring intensifies free-surface oscillations and modifies the internal pressure-amplification characteristics.

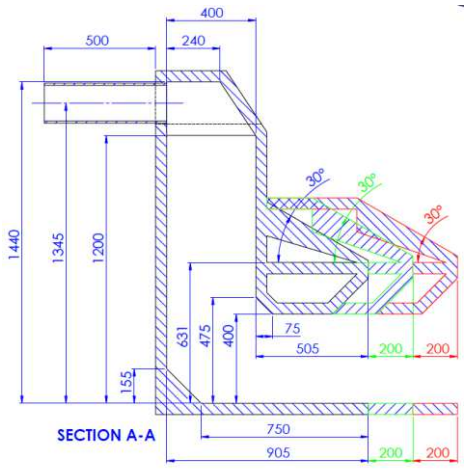


Figure 1. Section A–A of the L-OWC chamber

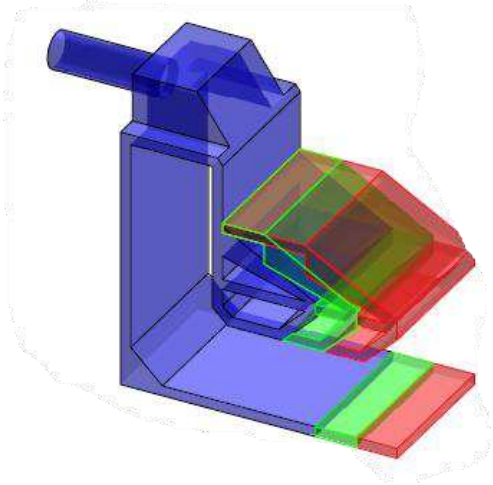


Figure 2. The L-OWC 3D model

To assess geometric sensitivity, two alternative horizontal duct lengths were evaluated. These variations were implemented by extending or shortening the horizontal chamber section while keeping all other structural parameters constant. This approach isolates the influence of the horizontal duct length on water-column displacement, internal pressure distribution, and the dynamics of the enclosed air volume. Features such as the throat width (0.075 m), roof inclination, and stepped inner profiles were maintained across all test cases to avoid introducing confounding geometric effects.

The selection of the L-shaped configuration was motivated by prior evidence indicating improved wave-energy capture and enhanced phasing between incident waves and internal oscillations. The stepped and inclined internal surfaces were designed to adjust the effective air-pocket volume and promote more pronounced piston-like water-column motion, which is essential for efficient energy conversion in OWC systems. The scaled model allowed a systematic examination of these geometric influences under controlled wave conditions, providing prototype-relevant insights into the relationship between chamber configuration and oscillatory performance.

The wave-to-pneumatic conversion efficiency was evaluated as the ratio of mean pneumatic power delivered to the air chamber to the incident wave power, which induces periodic compression and expansion of the air chamber. The conversion efficiency is defined as bellow :

$$\eta_{wp} = \frac{\bar{P}_{pneumatic}}{\bar{P}_{wave}} \quad (1)$$

P wave is incident wave power, P pneumatic is the time-averaged pneumatic power obtained from the chamber pressure and airflow rate.

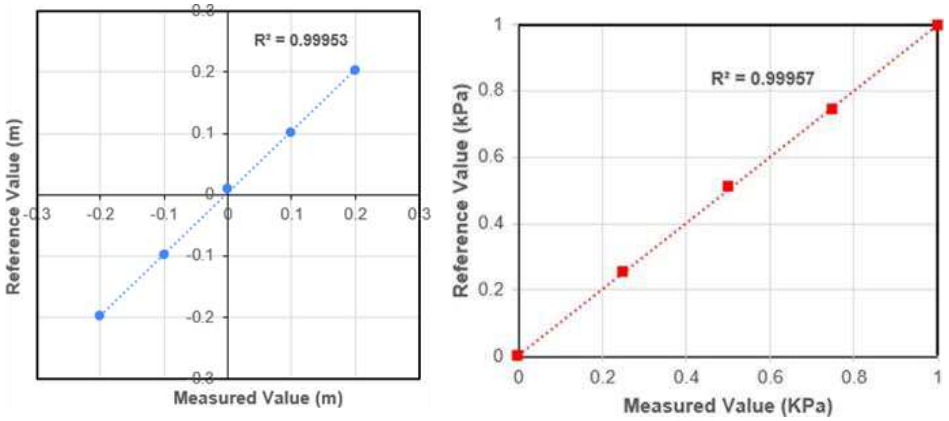
2.3. Instrumentation

For wave measurements, seven resistance-type wave gauges were deployed along the flume. One gauge was positioned 1.0 m in front of the wavemaker to characterize the incident wave field, while four gauges were installed on the seaside of the L-OWC model to enable the computation of incident, reflected, and transmitted components through multi-point decomposition. Two additional gauges were mounted inside the chamber to monitor free-surface oscillations and to provide independent verification of the chamber resonance response. The selected spacing between gauges ensured that phase differences remained within the linear reconstruction limits recommended by IAHR and the Ocean Energy Systems (OES) guidelines.

To complement the wave measurements, seven piezo-resistive pressure transducers were installed to record temporal pressure fluctuations. Two transducers were mounted inside the chamber to capture the dynamic pressure associated with the OWC. Five additional transducers were placed along the turbine duct: PS8 measured the static pressure upstream of the turbine plane, PS5 recorded the total pressure in the outflow direction, and PS6 measured the total pressure in the inflow direction to evaluate air decompression effects. PS3 and PS7 were positioned within the duct to resolve the internal pressure gradient, enabling air-velocity estimation using a Bernoulli-based

formulation. The positions of the sensors were selected to ensure adequate resolution of the spatial pressure distribution and to avoid local flow disturbances near geometric transitions.

All wave and Pressure Sensors (PS) were sampled at 40 Hz, a frequency selected to capture at least twenty times the highest expected harmonic associated with chamber resonance and wave–structure interaction. Prior to testing, each device underwent static and dynamic calibration following ISO 17025 procedures, including assessment of linearity, repeatability, zero drift, and phase lag. Calibration curves were used to correct sensor outputs during post-processing.



(a)

Figure 3. Calibration curves of WG and PS with corresponding R^2 values

Before testing, all measurement tools were calibrated to guarantee reliable data collection. This investigation employed resistive-typeWG with a measuring accuracy of ±0.5 mm. With an accuracy of ±0.5% of the full-scale range, the PS were piezoresistive flush-face sensors. Controlled input signals were used to perform linear calibration processes for each sensor. With coefficients of determination (R^2) ranging from 0.9995 to 0.9999, the calibration findings demonstrated outstanding linearity for both WG and PS that it can be seen in Fig.3.

Wave-generation durations of 60–120 s were employed to ensure that each run contained a sufficient number of steady-state wave cycles for statistical convergence. This approach follows the OES guidelines and recommendations in the *Handbook of Ocean Wave Energy*, which emphasize the need for sufficiently long records to suppress transient start-up effects and minimize spectral distortion. The model was positioned at a distance consistent with Hydralab III protocols to reduce secondary disturbances and ensure that the incident waves approached the L-OWC structure with minimal contamination.

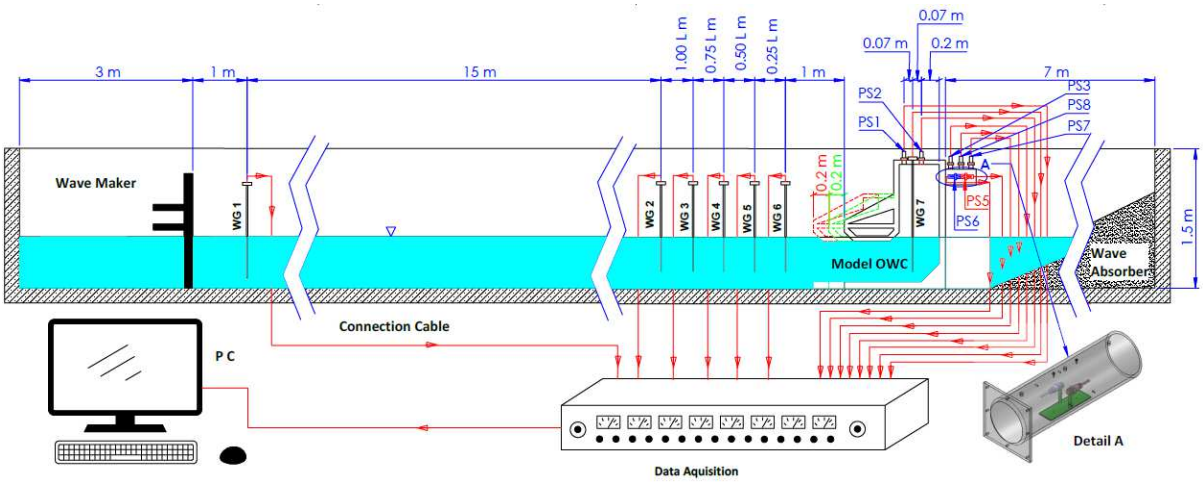


Figure 4. Operating Procedures for Flume Laboratories

All sensors were interfaced with a centralized multi-channel data acquisition system (DAQ), enabling fully synchronized acquisition of wave elevation, pressure, and airflow-related signals. Data were continuously sampled at 40 Hz for each run, with a recording duration of 110 s for regular waves. The acquired data were

subsequently processed to determine wave reflection and transmission coefficients, chamber oscillation amplitudes, pressure fluctuations, and air-flow characteristics using phase-averaged and spectral analysis methods, this configuration can be seen in Fig.4.

2.4. Experimental parameters and variables

Detail of the experimental parameters and variables are summarized in Table 1. Single wave height was evaluated, which was 0.025 m. These were obtained from variation of nine periods and three various sizes of geometries, single water depth,which was 0.75 m, and type of wave is generated regular waves.

Table 1. Experiment parameters and variables

Parameters	Variables
Test series generated by wavemaker	Period/T (s) and Wave Height/H(m)
	Period (s) =
	2.06; 2.37; 2.69; 3.0; 3.32; 3.64; 3.95; 4.27;4.59
	Wave height/ H (m) = 0.225
Length sizes of horizontal columns	Geometry 1 (Geo 1)
	Geometry 2 (Geo 2)
	Geometry 3 (Geo 3)
Scale	1:10
Turbine duct size (m)	0.16
Water depth (m)	0.75
Type of wave	Regular wave

2.5 Dimensional and Non-Dimensional Analysis

Most hydrodynamics analysis of OWC systems are grounded in Airy's linear wave theory, which assumes small-amplitude,irrotational, and inviscid flow conditions. Within this theoretical framework based on (Rodríguez et al., 2020), the relationship between the angular frequency (ω), wave number (κ), gravitational acceleration (g), and water depth (h) is defined by the linear wave dispersion relation, it can be seen on Eq.1

$$\omega^2 = gk\ tan\ tan\ h\ (kh) \tag{2}$$

Here, $k = \frac{2\pi}{\lambda}$ represents the wave number, $\omega = \frac{2\lambda}{T}$ is the angular frequency, T denotes the wave period, g is the gravitational acceleration and h is the water depth. This equation forms the theoretical foundation (Bingham et al., 2015, 2025; Supriyanto et al., 2025) for calculating the wavelength (λ) under various hydrodynamic conditions.

In addition to the external wave forcing, the OWC chamber exhibits an intrinsic natural frequency governed by the coupled dynamics of the water column and the trapped air volume. The system can be approximated as a linear mass–spring oscillator, where the water column provides inertia and the restoring force arises from both gravity and air compressibility. Under linear assumptions, the natural angular frequency can be expressed as (e.g., Bingham et al., 2015):

$$\omega_n = \sqrt{\frac{g}{L_e} + \frac{\gamma\ P_0\ A_\omega}{\rho\ L_e\ V_0}} \tag{3}$$

where Le is the effective water-column length and V_0 is the chamber air volume. The corresponding natural period is $T_n=2\pi/\omega_n$. This relation shows that chamber geometry directly controls resonance through the oscillating length and enclosed air volume. Resonance amplification occurs when the incident wave period approaches the natural period ($T \approx T_n$), enhancing both hydrodynamic motion and pneumatic response.

If air compressibility is neglected, the pneumatic stiffness vanishes and the system reduces to a gravity-controlled oscillator:

$$\omega_n = \sqrt{\frac{g}{L_e}}, \; T_n = 2\pi\sqrt{\frac{L_e}{g}} \tag{4}$$

In this limiting case, resonance depends solely on the water-column length, highlighting the critical role of air compressibility in modifying OWC dynamics and energy conversion (Bingham et al., 2015).

The dispersion relation can be arranged into the nonlinear implicit form:

$$\lambda = \frac{gT^2}{2\pi} tan\ tan\ h\ \frac{2\pi h}{\lambda} \tag{6}$$

which is typically solved using iterative or numerical methods. This formulation describes how the wavelength depends on both the period and the relative water depth. In the experimental and numerical investigations, Schaffer's correction is applied to the Airy model to mitigate the influence of wave reflection and to enhance the accuracy of wave generation (Schaffer, n.d.). By incorporating this correction, the wave profile generated in laboratory flumes or numerical wave tanks can more accurately reproduce target wave conditions predicted by the dispersion relation above. From a dimensional analysis perspective, the key non-dimensional parameter governing wave behaviour include:

$$kh, \qquad \frac{H}{\lambda}, \qquad \frac{gT^2}{h} \tag{7}$$

where the parameter kh (dimensionless depth) distinguishes between deep, intermediate, and shallow water regimes.

The ratio $\frac{H}{\lambda}$ represents wave stepness, including nonlinearity and potential wave breaking. Together, these non-dimensional quantities provide a systematic basis for scaling experimental data, comparing model and prototype conditions, and validating numerical simulations of OWC hydrodynamics.

Wave gauge (WG) 7 was installed within the chamber to record the oscillatory behaviour of the FSE(see Fig. 1). Apart from the WGs, five PS were placed inside the turbine duct and two PS sensors were placed inside the chamber. PS 3, PS 5, PS 6, PS 7, and PS 8 were installed perpendicular to the direction of the airflow, while PS 1 and PS 2 were positioned inside the chamber to measure the air pressure. In this study, two approaches were used to measure the OWC power. Using PS, the first approach measured the airflow velocity inside the turbine duct. To measure the overall pressure, PS 5 and PS 6 were placed in the middle of the turbine duct. PS 5 recorded the overall pressure leaving the chamber, while PS 6 measured the pressure entering the chamber. PS 8 was installed to measure the static pressure on the turbine duct wall. The OWC power produced in the Powc-duct turbine duct can be stated as follows:

$$P_{OWC} = \frac{1}{2}\rho\, A\, v^3 \tag{8}$$

$$v_\alpha = \sqrt{\frac{2}{\rho}(P_{total} - P_{static})} \tag{9}$$

Where P_{OWC} express the power produced within the turbine duct, A is the perpendicular area of the turbine duct, and v is the airflow velocity input and output from the turbine duct.

The following definitions apply to a chamber's non-dimensional wave surface elevation amplitude (A_η^*), air pressure amplitude (A_{ap}^*), and air volume amplitude (A_V^*) (Palmer et al., 2023):

$$A_\eta^* = \frac{\eta_{max} - \eta_{min}}{H} \tag{10}$$

$$A_{pa}^* = \frac{Pa_{max} - Pa_{min}}{\rho g H} \tag{11}$$

and

$$A_V^* = \frac{V_{max} - V_{min}}{WlH} \tag{12}$$

Where W is the width of the flume, l is the length of the OWC chamber, and H is the wave height. The maximum and minimum values of the corresponding variable within a single wave period are indicated by the subscripts max and min, respectively.

From a physical perspective, the OWC chamber can be idealised as a coupled mass-spring-damper system, where the OWC provides the inertial mass, gravity and air compressibility provide the restoring stiffness, and radiation losses together with viscous dissipation constitute the damping mechanism. In this framework, the chamber geometry directly controls the effective oscillating water mass through the duct length and wetted volume, while the enclosed air volume determines the pneumatic stiffness through compressibility. Consequently, the natural frequency of the system is geometry-dependent. When the incident wave frequency approaches this natural frequency, resonance amplification occurs, increasing the free-surface oscillation amplitude and air-pressure response. However, the energy conversion efficiency depends not only on resonance amplitude but also on the phase relationship between water-column displacement, chamber pressure, and airflow velocity. Excessive radiation damping or nonlinear viscous losses can reduce this coherence and limit pneumatic power extraction even under resonant excitation.

3. Results and discussion

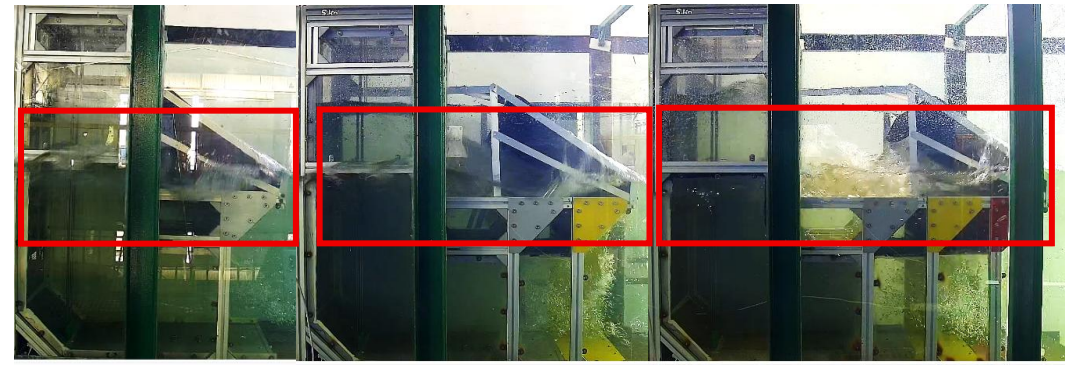
3.1. Hydrodynamics in the OWC Chamber

The primary hydrodynamic response inside the OWC chamber under regular wave excitation is the free-surface elevation (FSE), which represents the oscillatory motion of the internal water column and directly governs the induced airflow toward the turbine. For the present wave condition (H = 0.225 m, T = 2–3 s), the FSE responses of Geo 1, Geo 2, and Geo 3 exhibit distinct trends, reflecting the strong influence of chamber geometry on oscillation amplitude, coherence, and stability, as shown in Fig. 4 and Fig. 5(a–f).

Based on the time-averaged peak values extracted from Fig. 5(a), the maximum absolute FSE inside the chamber reaches approximately 0.80 m at T ≈ 2.75 s, corresponding to a non-dimensional free-surface elevation of $A_\eta^* \approx 3.56$ when normalised, based on Eq.7. Across the examined period range, Geo 3 generally exhibits the largest instantaneous FSE amplitudes, with values varying between ≈ 0.50–0.80 m ($A_\eta^* \approx 2.2$–3.6). However, this strong response is accompanied by pronounced temporal fluctuations, splashing, and disturbed free-surface motion near the inclined duct, indicating significant nonlinear effects such as wave steepening, vortex formation, and turbulence-induced dissipation.

Geo 1 shows moderately high FSE amplitudes (≈ 0.55–0.70 m, $A_\eta^* \approx 2.4$–3.1), but with noticeable variability over the wave cycle. Despite identical regular wave forcing, the irregular FSE response in Geo 1 suggests the presence of higher-order harmonics, internal sloshing modes, and possible mode coupling within the chamber. These nonlinear dynamics distort the near-sinusoidal piston motion of the water column, leading to unstable pressure oscillations and unsteady air displacement, which are detrimental to pneumatic efficiency.

In contrast, Geo 2 demonstrates the most stable and coherent FSE response, with amplitudes remaining within ≈ 0.55–0.72 m ($A_\eta^* \approx 2.4$–3.2) across the investigated period range. Although its peak amplitude is slightly lower than that of Geo 3, Geo 2 exhibits a smoother piston-type oscillation with limited splashing and reduced temporal variability. This behaviour indicates operation close to a quasi-resonant condition, where favourable phase alignment between the incident wave excitation and internal water-column motion is achieved. Such coherence is essential for maintaining stable chamber pressure oscillations and sustaining efficient airflow through the turbine duct. The observed FSE behaviour, particularly the stable piston-type oscillation in Geo 2 and the amplified response near the resonant condition, is consistent with predictions from linear wave theory and with experimental observations reported in previous OWC studies, such as (Rezanejad et al., 2019). This agreement confirms that the present experimental setup is capable of accurately reproducing the hydrodynamic response of OWC systems under near-resonant wave conditions.



(a) (b) (c)



(d) (e) (f)

Figure 5. Test scenario H=0.225 m; T=2-3.5 s
(a), (b), (c) High Oscillations of FSE and
(d), (e), (f) Low Oscillations of FSE.

Observations from Fig. 5 further reveal that chamber height plays a crucial role in shaping the FSE response. The high-chamber configuration exhibits stronger vertical oscillations but also greater sensitivity to nonlinear fluctuations, while the low-chamber configuration promotes lateral overflow and enhanced wave reflection, which suppresses effective vertical water-column motion. These findings confirm that the OWC chamber does not function merely as a passive air–water interface, but rather as a hydrodynamic filter that selectively amplifies or attenuates components of the incoming wave energy depending on its geometric characteristics.

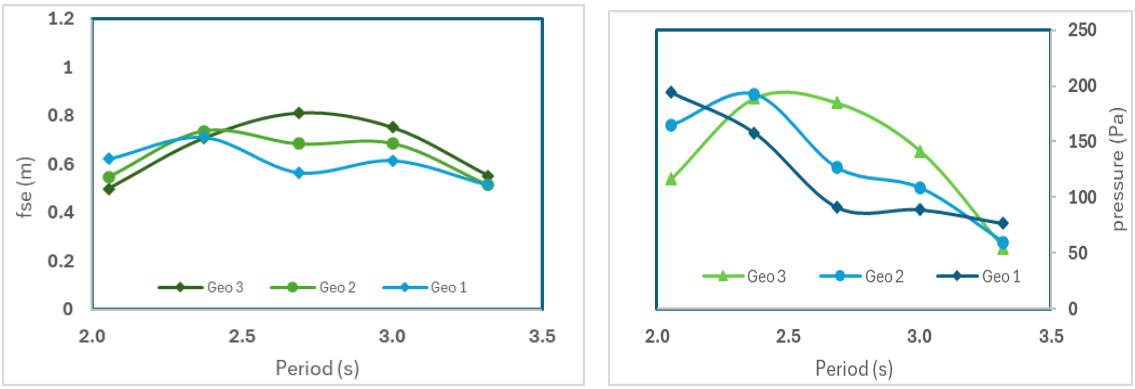
The comparative analysis shown in Fig. 6 (a) highlights that large FSE amplitudes alone do not guarantee superior energy conversion performance. While Geo 3 produces the strongest instantaneous free-surface agitation, a significant fraction of the wave energy is dissipated through turbulent and incoherent motion. Geo 1 suffers from similar limitations due to nonlinear instability. Geo 2 achieves the most favourable balance between excitation magnitude and oscillatory stability, enabling more effective hydrodynamic-to-pneumatic energy transfer. These results underscore the importance of geometry optimisation grounded in both nonlinear wave mechanics and multiphase hydrodynamic theory to enhance the performance of OWC wave-energy converters.

3.2. Chamber Pressure Response

The pressure distributions shown in Fig. 6 (b) illustrate the coupling between the oscillatory motion of the internal water column and the compression-expansion behaviour of the trapped air within the OWC chamber under regular wave conditions with a wave height of H = 0.225 m and wave periods ranging from T = 2.0 to 3.0 s. This coupling is a defining characteristic of OWC systems, as variations in FSE directly induce volumetric air displacement and corresponding pressure fluctuations. Geo 1 exhibits relatively high-pressure values at shorter periods, with pressures of approximately 210–220 Pa at T = 2.0 s, followed by a pronounced reduction to around 150 Pa at T = 2.5 s and further decreasing to approximately 90–100 Pa at T = 3.0 s. This sharp decline suggests strong sensitivity of the pressure response to wave period, potentially associated with nonlinear excitation and increased internal dissipation as the system moves away from its favourable oscillatory range.

Geo 3 produces moderate to high pressure levels with noticeable variability across the same period range. The pressure increases from approximately 130 Pa at T = 2.0 s to a peak of about 185–190 Pa at T = 2.5 s, before decreasing to roughly 140 Pa at T = 3.0 s. Although Geo 3 achieves relatively high peak pressure, the broader spread and less uniform trend indicate instability in the pressure response, which may arise from irregular internal flow patterns or suboptimal alignment between the incident wave forcing and the chamber's natural oscillatory

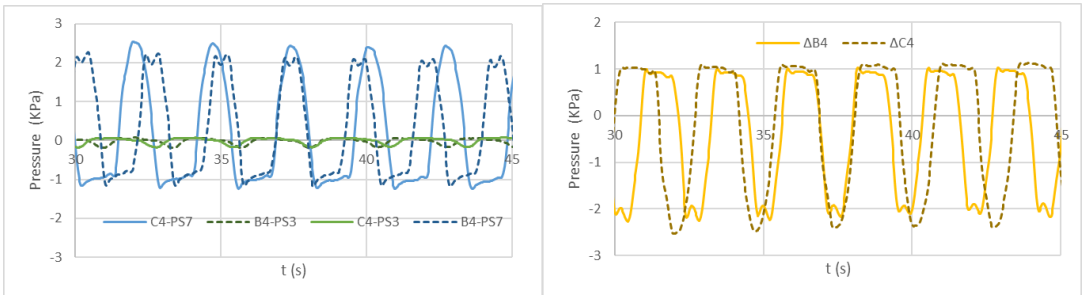
modes. Such behaviour suggests that a portion of the available wave energy is dissipated through internal turbulence rather than contributing to coherent pneumatic compression.



(a) (b)

Figure 6. Variation of (a) FSE and (b) pressure against wave period for Geo 1, Geo 2, and Geo 3

In contrast, Geo 2 demonstrates the most uniform and phase-consistent pressure response among the three geometries. The pressure rises smoothly from approximately 170–180 Pa at T = 2.0 s to a peak of about 200 Pa at T = 2.5 s, followed by a gradual decrease to around 120–130 Pa at T = 3.0 s. This regular pressure evolution indicates a stable balance between excitation force and radiation impedance, minimising phase lag and suppressing chaotic flow structures within the air chamber. Such stability is favourable for pneumatic energy conversion, as it promotes smoother airflow toward the turbine, reduces turbulence-induced dissipation, and supports a more predictable mass-flow rate. Meanwhile, Geo 1 and Geo 3 show higher sensitivity to wave period and greater pressure distortion under H = 0.225 m, Geo 2 achieves the most robust and reliable pressure response, highlighting the importance of geometric optimisation that prioritises pressure stability in addition to amplitude amplification. The measured pressure trends and their dependence on wave period and chamber geometry are in good agreement with previously reported experimental findings, where pressure stability and phase consistency were identified as key factors governing pneumatic efficiency in OWC systems, as discussed by (Ning et al., 2019). This consistency supports the reliability of the present pressure measurements and their physical interpretation. To further support the interpretation of the pressure behaviour within the chamber, a detailed analysis of the spatial pressure variation along the air duct is performed based on time-series measurements. The pressure signals recorded at two locations, PS3 and PS7, are presented in Fig. 7 (a). The results reveal a clear difference in both amplitude and phase between the two signals, indicating that the pressure response is not spatially uniform even within a relatively short duct length of 0.16 m. This behaviour reflects the dynamic interaction between the oscillating air mass and the internal flow resistance, which induces a measurable pressure gradient along the duct. Furthermore, the corresponding pressure difference, defined as ΔP = PS3 – PS7, is shown in Fig. 7 (b). The ΔP signal exhibits a consistent non-zero oscillatory pattern over time, confirming the existence of a pressure drop between the two measurement locations. The persistence of this pressure difference throughout successive wave cycles demonstrates that the measurement system is sufficiently sensitive to capture spatial pressure variations despite the compact geometry of the duct. These findings validate the use of distributed PS for quantifying internal pneumatic behaviour and provide additional evidence of energy dissipation mechanisms within the OWC system.

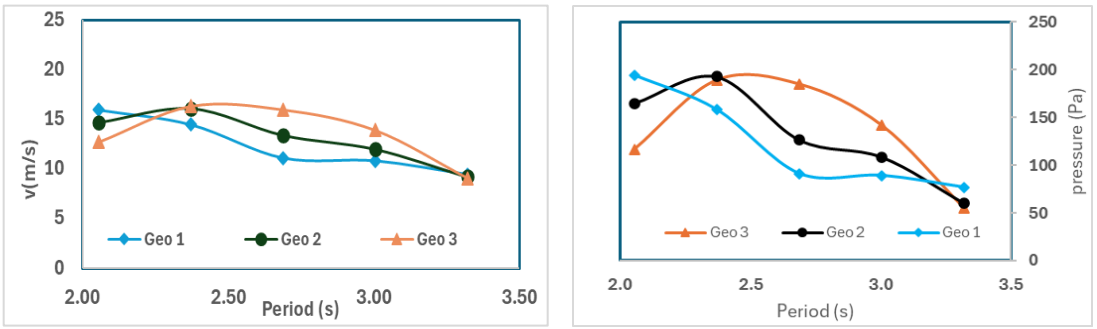


(a) (b)

Figure 7. (a) Variation of PS 3 & 7 and (b) ΔP

3.3. Velocity Distribution within the Chamber

The Fig. 8 (a) presents the velocity distribution within the OWC chamber under regular wave conditions with a wave height of H = 0.225 m and wave periods ranging from T = 2.0 to 3.0 s. The results clearly demonstrate that chamber geometry plays a decisive role in governing internal velocity magnitude and stability. Geo 2 exhibits the most stable velocity response across the investigated period range, with velocities increasing from approximately 14.5 m/s at T = 2.0 s to a peak of about 16.0 m/s at T = 2.5 s, before gradually decreasing to around 12.0 m/s at T = 3.0 s. This smooth trend indicates coherent air displacement driven by a well-synchronised oscillation of the internal water column.



(a) (b)

Figure 8. Variation of (a) velocity and (b) pressure against wave period for Geo 1, Geo 2, and Geo 3

In contrast, Geo 1 shows significant velocity fluctuations, with values decreasing sharply from about 16.0 m/s at T = 2.0 s to approximately 11.0 m/s at T = 2.5 s, and remaining relatively low near 10.5–11.0 m/s at T = 3.0 s. Such abrupt changes suggest the presence of flow separation or localised turbulence induced by geometric constraints within the chamber. Geo 3 produces moderate velocity levels, increasing from around 12.5 m/s at T = 2.0 s to a maximum of approximately 16.0 m/s at T = 2.5 s, followed by a reduction to about 14.0 m/s at T = 3.0 s. However, despite its relatively high peak velocity, Geo 3 exhibits less consistency than Geo 2, indicating partial inefficiency in guiding internal flow.

Since internal air velocity directly governs the instantaneous mass flow rate entering the turbine, these differences carry important implications for pneumatic performance. The stable and phase-consistent velocity profile of Geo 2 suggests minimised flow separation and reduced viscous dissipation, enabling more efficient conversion of pneumatic energy into mechanical output. In contrast, the irregular velocity patterns observed in Geo 1 and the intermittent disturbances in Geo 3 may lead to unsteady mass-flow conditions, pressure distortion, and increased aerodynamic losses. Although Geo 3 achieves relatively high instantaneous velocities, its reduced coherence limits effective energy transfer. Overall, Geo 2 demonstrates the most favourable balance between velocity magnitude and stability, highlighting the importance of geometric optimisation in promoting coherent airflow within OWC chambers under regular wave excitation.

3.4. Power Output

The implications of the hydrodynamic and pneumatic distinctions among the three geometries become more evident when the resulting non-dimensional power output is examined, as illustrated in the radar chart. The power output of an OWC system is governed by the instantaneous product of the pressure differential and volumetric airflow rate, thus representing an integrated response of free-surface elevation, internal pressure oscillation, and air-velocity coherence. For the present wave condition (H = 0.225 m, T = 2–3 s), all performance indicators are normalised with respect to the maximum observed response, yielding non-dimensional values ranging from 0 to 1.00.

Based on the radar chart in Fig. 9, Geo 2 exhibits the highest and most balanced non-dimensional power-related response, with values clustering in the range of approximately 0.70–0.85 across the dominant parameters. In particular, the non-dimensional indicator associated with power output for Geo 2 reaches about 0.80, exceeding that of Geo 1 (≈ 0.65) and Geo 3 (≈ 0.55). This indicates that Geo 2 most effectively converts the available wave-induced hydrodynamic energy into usable pneumatic power under intermediate wave periods.

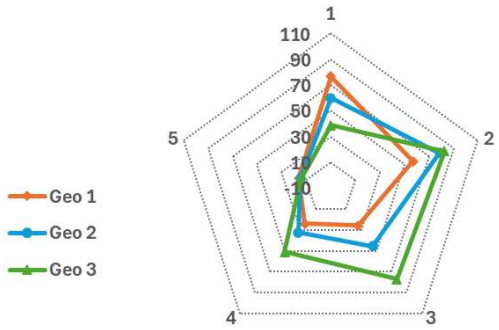


Figure 9. Relationship between power output and period on Geo 1, Geo 2, and Geo 3

The superior performance of Geo 2 can be attributed to its stable pressure–velocity coupling, as reflected by its moderate-to-high free-surface response (≈ 0.75) combined with coherent airflow characteristics (≈ 0.80). The near-harmonic alignment between water-column oscillation and induced airflow suggests a favourable phase relationship, enabling the pneumatic work performed on the turbine to approach its optimal value during each wave cycle. Consequently, destructive phase lag between pressure peaks and airflow momentum is minimised, allowing Geo 2 to maintain a consistently high-power extraction level throughout the oscillation period.

In contrast, Geo 1, while exhibiting relatively strong hydrodynamic excitation evidenced by a higher non-dimensional free-surface motion and pressure amplitude (up to ≈ 0.85) fails to translate this forcing into proportional power output. Its non-dimensional power metric remains limited to around 0.65. This discrepancy is primarily associated with internal flow irregularities, including velocity fluctuations and turbulence-induced disturbances, which reduce the effective volumetric airflow rate. As a result, a portion of the available pressure energy is dissipated internally through vorticity and unsteady pressure fields rather than being converted into useful mechanical power.

Geo 3, on the other hand, consistently records the lowest non-dimensional amplitudes across the evaluated parameters. Its free-surface response and pressure oscillation remain below ≈ 0.60, leading to a non-dimensional power output of only ≈ 0.55. Although the internal flow appears more stable than that of Geo 1, the reduced excitation indicates that the chamber geometry dampens incoming wave energy, flattening the oscillatory response and limiting airflow magnitude. This trade-off between dynamic stability and energy engagement results in the weakest power performance among the three configurations.

The chart clearly demonstrates that maximum power output is not achieved solely through high hydrodynamic forcing, but rather through an optimal balance between excitation amplitude, pressure stability, and airflow coherence. Under the examined wave conditions (H = 0.225 m, T = 2–3 s), Geo 2 provides the most favourable non-dimensional power output, highlighting the critical role of geometry-induced phase synchronisation in enhancing OWC energy conversion efficiency.

3.5. Physical Mechanism Linking Geometry to Power Output

The primary mechanism connecting chamber geometry to pneumatic power output is a resonance-driven hydrodynamic-pneumatic coupling, influenced by air compressibility and radiation damping. All configurations were tested under near-resonant wave conditions, and the results show that efficient power extraction doesn't just depend on the size of the free-surface oscillations. It also depends on how stable and in phase the water-column motion and air-pressure response are. In Geometry 2, the internal water column oscillation is almost in resonance with the compressible air dynamics. This makes the pressure oscillations stable and the airflow efficient. Geometry 1 and Geometry 3, on the other hand, do not follow this best coupling because of nonlinear sloshing, phase mismatch, and more energy loss. Therefore, the observed behaviour can be considered resonance-driven, but strongly governed by geometry-dependent phase alignment and damping effects.

3.6. Comparison between Non-Dimensional Variables

The comparative evaluation of the non-dimensional free-surface elevation amplitude ($A_{(}fse_{)}$) among the three geometries reveals pronounced differences in hydrodynamic response under the examined wave condition (H = 0.225 m, T = 2–3 s), as shown in Fig. 10. Across the investigated range of kH ≈ 0.6–1.0, Geo 1 consistently exhibits the highest $A_{(}fse_{)}$, reaching peak non-dimensional values of approximately 2.8–3.1 around kH ≈ 0.6–0.7, before gradually decreasing toward ≈ 2.7 at kH ≈ 1.0. These elevated amplitudes indicate strong wave excitation and substantial water-column motion. However, the noticeable variability of $A_{(}fse_{)}$ suggests the presence of nonlinear hydrodynamic responses, including amplitude modulation, internal sloshing, and potential mode-coupling effects, which inhibit the development of a stable harmonic oscillation. Consequently, the high

hydrodynamic excitation in Geo 1 does not guarantee effective pneumatic energy conversion, as irregular free-surface motion tends to induce fluctuating and unstable pressure gradients within the chamber.

In contrast, Geo 2 maintains moderate yet highly consistent $A_{(fse)}$ values, generally confined within ≈ 2.3–3.0 over the same kH range. The reduced scatter and smoother trend imply that the geometry successfully balances wave-energy absorption and hydrodynamic stability. Such behaviour is particularly advantageous for OWC systems, as a predictable free-surface oscillation supports regular air compression–expansion cycles and minimises turbulence-induced losses. Geo 3, meanwhile, demonstrates the lowest effective hydrodynamic engagement, with $A_{(fse)}$ peaking at ≈ 3.4–3.6 around kH ≈ 0.7, but rapidly declining to ≈ 2.2 at kH ≈ 1.0. This narrow dynamic range indicates that Geo 3 does not maintain effective coupling with the incident wave field across varying conditions, thereby limiting its air-displacement capability.

A comparable trend is observed in the non-dimensional pressure amplitude (A_p), as depicted in Fig. 11. Geo 2 again displays the most favourable pressure behaviour, achieving peak A_p values of approximately 0.085–0.090 near kH ≈ 0.85, while maintaining relatively low variability across the investigated range. This stability is critical, as pneumatic conversion efficiency is strongly governed by the regularity of pressure oscillations that drive airflow through the turbine. Geo 1, although generating increasing pressure amplitudes with kH rising from ≈ 0.035 at kH ≈ 0.6 to ≈ 0.090 at kH ≈ 1.0 exhibits signs of instability associated with complex interactions between the oscillating free surface and the compressible air layer. These interactions may trigger nonlinear pressure spikes, quasi-turbulent flow behaviour, or internal resonance effects that compromise efficient airflow regulation. Geo 3, by comparison, reaches its maximum A_p of ≈ 0.085 at kH ≈ 0.7–0.8, but subsequently declines to ≈ 0.055 at kH ≈ 1.0, reflecting a conservative pneumatic response aligned with its subdued hydrodynamic excitation. The obtained non-dimensional parameters, including free-surface elevation amplitude and pressure amplitude, fall within the range reported in previous experimental and numerical investigations of OWC systems. Similar trends have been observed by (Elhanafi et al., 2018), where geometric variations influenced both hydrodynamic response and pressure stability. This agreement further validates the consistency of the present results with established OWC behaviour.

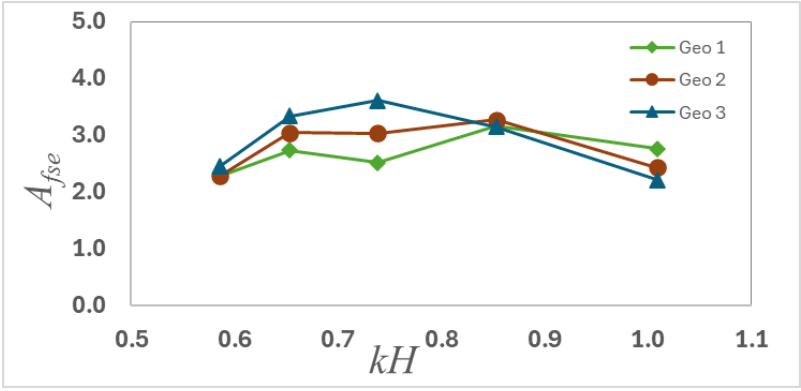


Figure 10. Relation between wave surface elevation amplitude and dimensionless depth

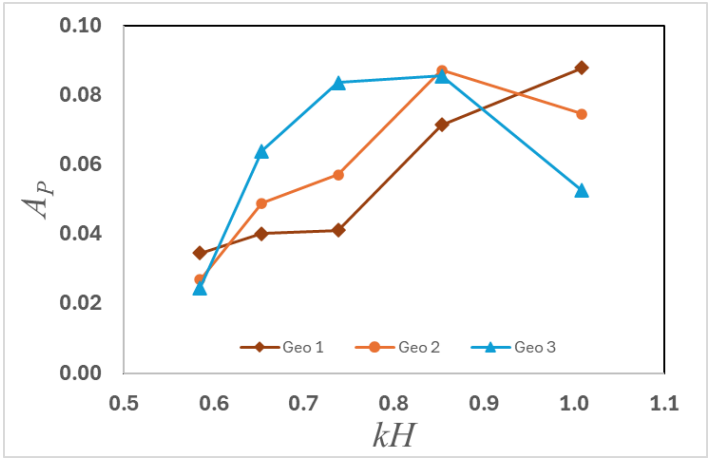


Figure 11. Relation between air pressure amplitude and dimensionless depth

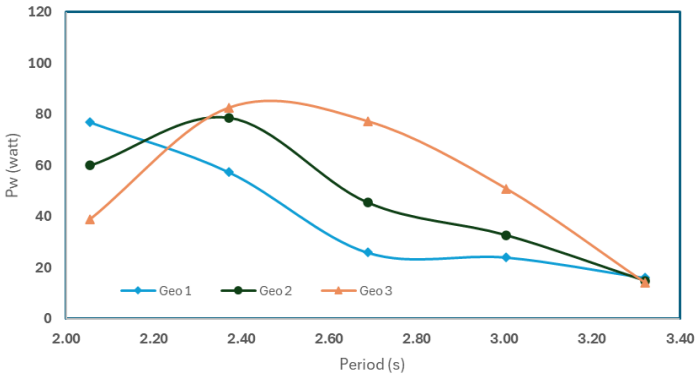


Figure 12. The relation between power and period

The observed geometry-dependent behaviour can be interpreted as a resonance-controlled hydrodynamic-pneumatic coupling process. The peak responses occurring at wave periods of approximately T ≈ 2.4 to 2.6 s indicate that all three geometries operate within a near-resonant regime, but with different effective natural periods due to differences in internal water-column length and chamber air volume. Geo 2 appears to achieve the most favourable tuning between incident-wave forcing and chamber natural frequency, resulting in strong but stable oscillations. This condition maximises constructive energy transfer into the air chamber and promotes efficient compression-expansion cycles. In contrast, Geo 1 exhibits stronger hydrodynamic excitation but larger radiation losses and internal flow separation, leading to partial decoupling between free-surface motion and pressure generation. Geo 3, while dynamically more stable, appears slightly detuned from the dominant wave forcing, producing lower effective resonance amplification. These results confirm that the dominant mechanism governing pneumatic power output is not simply amplitude amplification, but resonance-enhanced phase-coherent coupling between the hydrodynamic and pneumatic subsystems.

The sensitivity of Geo 1 and Geo 3 to resonance-prone wave conditions at H = 0.225 m becomes particularly evident when the pressure and FSE responses are considered together. Near-resonant forcing amplifies nonlinear interactions within these geometries, potentially generating exaggerated dynamic responses or measurement anomalies that obscure true performance trends. This underscores the necessity of careful data validation when assessing OWC behaviour under intermediate-to-high excitation levels.

The implications of these non-dimensional hydrodynamic and pneumatic characteristics are ultimately reflected in the power output trends, shown in Fig. 12. Within the examined period range (T = 2–3 s), Geo 2 consistently delivers the highest power output, peaking at approximately 80 W around T ≈ 2.4 s, and maintaining relatively high values (≈ 45–75 W) across the operational band. This superior performance confirms that the moderate but stable $A_{(}fse_{)}$ and A_p responses of Geo 2 facilitate efficient energy transfer from the water column to the pneumatic subsystem. Geo 1, despite experiencing strong hydrodynamic forcing, produces lower power levels declining from ≈ 75 W at T ≈ 2.1 s to ≈ 25 W near T ≈ 2.8–3.0 s, due to significant pneumatic losses associated with unstable pressure and velocity fields. Geo 3 exhibits an intermediate behavior, achieving a maximum of ≈ 85 W at T ≈ 2.4 s, but suffering a sharp reduction at longer periods as hydrodynamic engagement weakens.

Taken together, these results emphasize that high non-dimensional amplitudes alone do not ensure superior OWC performance. Instead, optimal energy extraction requires a geometry that balances excitation magnitude with dynamic stability across both hydrodynamic and pneumatic stages. Geo 2 achieves this balance most effectively, whereas Geo 1 illustrates the penalties of excessive nonlinearity and Geo 3 highlights the limitations imposed by insufficient wave–structure coupling.

3.7. Geometry Optimization and Design Guideline

The comparative experimental results provide a structured basis for identifying the optimal chamber geometry and deriving practical design guidelines for L-shaped OWC systems. Although all three configurations operate within a near-resonant wave regime, their performance differs substantially due to geometry-dependent variations in hydrodynamic stability, pressure build-up, and airflow coherence.

Among the tested configurations, Geo 2 emerges as the optimal chamber design because it achieves the most balanced performance across all measured parameters. Unlike Geo 1, which produces high free-surface amplitudes but suffers from internal flow instability and pressure irregularity, and Geo 3, which exhibits lower hydrodynamic engagement outside a narrow operational range, Geo 2 maintains stable piston-like water-column motion, coherent chamber-pressure oscillations, and sustained airflow velocity over the investigated wave periods. This balanced response leads to the highest sustained pneumatic power output and the most reliable energy conversion performance.

The optimisation results indicate that effective OWC chamber design should not aim solely to maximise hydrodynamic amplitude. Instead, three geometry-selection criteria should be prioritised. First, the chamber geometry should maintain stable piston-mode oscillation while minimising sloshing and turbulence-induced dissipation. Second, the chamber air volume should be sufficiently tuned to generate strong but stable pressure amplification without excessive compressibility-induced phase lag. Third, the horizontal duct length should be selected to align the natural period of the coupled water-column–air system with the dominant incident wave period, thereby achieving near-resonant operation.

These findings establish a practical design guideline for future L-OWC development: the optimal chamber configuration is the one that maximises phase-coherent hydrodynamic–pneumatic coupling rather than simply maximising oscillation amplitude. Within the tested design space, Geo 2 satisfies this criterion most effectively and is therefore recommended as the reference geometry for future scale-up and turbine integration studies.

4. Conclusion

From an optimisation perspective, Geo 2 is identified as the optimal configuration among the tested geometries, consistently achieving the best balance between hydrodynamic amplification, pressure stability, airflow coherence, and sustained pneumatic power output. The results demonstrate that OWC performance under intermediate wave conditions (H = 0.225 m, T = 2 to 3 s) is governed primarily by the coherence between hydrodynamic excitation and pneumatic response, rather than by oscillation amplitude alone.

Comparative analysis of free-surface elevation, pressure oscillation, and power output shows that Geo 2 outperforms the other configurations by maintaining moderate yet stable oscillations, enabling effective pressure–velocity coupling and sustained airflow. In contrast, Geo 1, despite exhibiting the highest amplitudes, suffers from nonlinear instabilities that reduce pneumatic efficiency, while Geo 3 provides insufficient excitation for effective energy extraction.

These findings confirm that optimal OWC performance is achieved through a balance between excitation strength and dynamic stability, rather than maximising amplitude alone. Chamber geometry plays a fundamental role by controlling the system's effective inertial mass, pneumatic stiffness, and damping, thereby determining the natural frequency and phase relationship between hydrodynamic forcing and pneumatic conversion. The superior performance of Geo 2 indicates that maximum power extraction occurs under near-resonant conditions where pressure amplification and airflow coherence are simultaneously optimised.

The sensitivity of Geo 1 and Geo 3 to near-resonant excitation further highlights the importance of careful data validation under resonance-prone conditions. Although this study is based on regular waves, the observed geometric effects are expected to remain qualitatively valid in real sea states, where additional nonlinear and spectral effects may influence performance.

Overall, this study underscores the importance of geometry-informed design for efficient OWC systems. Future work will extend the analysis to irregular wave conditions, incorporate turbine–chamber interactions, and employ high-fidelity coupled air–water simulations alongside experimental validation to identify optimal operating regimes.

Funding

The authors declare that no funds, grants, or other support were received for conducting this study or for the preparation of this manuscript.

References

Bingham, H. B., Ducasse, D., Nielsen, K., & Read, R. (2015). Hydrodynamic analysis of oscillating water column wave energy devices. *Journal of Ocean Engineering and Marine Energy*, *1*(4), 405–419. https://doi.org/10.1007/s40722-015-0032-4

Bingham, H. B., Joensen, B., Read, R. W., Nielsen, K., Tran, T. T., Said, H. A., Kelly, T., Ringwood, J. V., Imai, Y., van der Zanden, J., Yu, Y. H., Eskilsson, C., & Shiri, A. A. (2025). Benchmark study of the DTU OWC chamber with both two-way and one-way absorption. *Journal of Ocean Engineering and Marine Energy*, *11*(3), 761–782. https://doi.org/10.1007/s40722-025-00384-y

Çelik, A., & Altunkaynak, A. (2020). Determination of hydrodynamic parameters of a fixed OWC by performing experimental and numerical free decay tests. *Ocean Engineering*, *204*. https://doi.org/10.1016/j.oceaneng.2019.106827

de Lima, Y. T. B., Isoldi, L. A., dos Santos, E. D., Machado, B. N., Gomes, M. das N., Biserni, C., & Rocha, L. A. O. (2024). Study of the Geometry of an Oscillating Water Column Device with Five Chambers Coupled under Regular Waves through the Constructal Design Method. *Fluids*, *9*(4). https://doi.org/10.3390/fluids9040086

EL Bouji, S., Kamil, N., & Beidouri, Z. (2023). Experimental study of an oscillating water column wave energy converter based on regular waves. *Marine Systems and Ocean Technology*, *17*(3–4), 147–163. https://doi.org/10.1007/s40868-022-00121-2

Elhanafi, A., Macfarlane, G., & Ning, D. (2018). Hydrodynamic performance of single–chamber and dual–chamber offshore–stationary Oscillating Water Column devices using CFD. *Applied Energy*, *228*, 82–96. https://doi.org/10.1016/j.apenergy.2018.06.069

Gadelho, J., Rezanejad, K., & Guedes Soares, C. (2024). Experimental and numerical analysis of multi-chamber oscillating water column devices. *Journal of Hydrodynamics*, *36*(3), 492–503. https://doi.org/10.1007/s42241-024-0043-5

Hendriyono, W., Wibowo, M., Saputri, A. N., Purwoko, A. S., Ratnasari, E., Wibowo, E. T., & Aziz, H. (2026). Preliminary assessment of nearshore wave energy in Morotai for remote electrification in Indonesia. *International Journal of Applied Science and Engineering*, *23*(1). https://doi.org/10.6703/IJASE.202603_23(1).004

Hsieh, M. F., Lin, I. H., Dorrell, D. G., Hsieh, M. J., & Lin, C. C. (2012). Development of a wave energy converter using a two chamber oscillating water column. *IEEE Transactions on Sustainable Energy*, *3*(3), 482–497. https://doi.org/10.1109/TSTE.2012.2190769

Juan, N. P., Valdecantos, V. N., Esteban, M. D., & Gutiérrez, J. S. L. (2022). Review of the Influence of Oceanographic and Geometric Parameters on Oscillating Water Columns. In *Journal of Marine Science and Engineering* (Vol. 10, Issue 2). MDPI. https://doi.org/10.3390/jmse10020226

Kim, J. S., Nam, B. W., Kim, S., Park, J., Park, S., & Kim, K. H. (2023). Experimental study on hydrodynamic behavior and energy conversion of multiple oscillating-water-column chamber in regular waves. *Ocean Engineering*, *280*. https://doi.org/10.1016/j.oceaneng.2023.114495

Kim, J.-S., & Nam, B. W. (2022). Numerical Analysis for Hydrodynamic Performance of OWC Devices with Multiple Chambers in Waves. *Journal of Ocean Engineering and Technology*, *36*(1), 21–31. https://doi.org/10.26748/ksoe.2021.091

Lin, C. C., Chow, Y. C., & Nguyen, D. T. (2023). The chamber design of the L-shaped oscillating water column using artificial neural network. *Proceedings of the European Wave and Tidal Energy Conference*. https://doi.org/10.36688/ewtec-2023-555

Marta, A. S. D., Deendarlianto, Kongko, W., Aprijanto, Rohman, A. T., Wibowo, A., & Ikhsanudin, I. Y. (2024). The influence of wave characteristics, tides, and installation conditions of L-shaped OWC wave energy converter on energy absorption capability. Evergreen, 11(3), 2607-2617. https://doi.org/10.5109/7236900.

Marta, A. S. D., Deendarlianto, Kongko, W., Indarto, Fauzun, & Rohman, A. T. (2024). The influence of wave height and period on airflow velocity and differential pressure in L-shaped oscillating water column (L-OWC) chamber for wave energy converter (WEC). Asia-Pacific Journal of Science and Technology, 29(6). https://doi.org/10.14456/apst.2024.90.

Marta, A. S. D., Sarjiya, Deendarlianto, Kamal, S., Indarto, & Winata, E. (2024). Performance of OWC-type wave power plants in the waters of Sumbawa Island, Indonesia. 2024 International Conference on Technology and Policy in Energy and Electric Power (ICTPEP), 415-420. https://doi.org/10.1109/ICT-PEP63827.2024.10733542.

Marta, A. S. D., Wibowo, A., Riyalda, B. F., Muttaqin, F. D., Fil Ardli, A. M. T., Rusdiutomo, A., Hendriyono, W., Hamid, A., Soesanto, Q. M. B., & Adiputra, R. (2026).* Performance of multi chamber oscillating water columns: Effects of chamber configuration and power absorption. Evergreen, 13(1), 173-187. https://doi.org/10.5109/7407643.

Malakani, A. I., Ikhsanudin, I. Y., Hendriyono, W., Rohman, A. T., Wibowo, A., Haq, J. A. K., Pratomo, T. B., Hakim, D. L., Musthofa, A., & Marta, A. S. D. (2026).* Impact of wave conditions on L-shaped oscillating water columns under irregular waves: A study considering Sumbawa, Indonesia's wave energy potential. Marine Systems & Ocean Technology, 21(4). https://doi.org/10.1007/s40868-025-00202-y.

Mandev, M. B., Altunkaynak, A., & Çelik, A. (2024). Enhancing wave energy harvesting: Performance analysis of a dual chamber oscillating water column. *Energy*, *290*. https://doi.org/10.1016/j.energy.2023.130191

Mocellin, A. P. G., Paiva, M. da S., dos Santos, E. D., Rocha, L. A. O., Isoldi, L. A., Ziebell, J. S., & Machado, B. N. (2024). Geometric Evaluation of an Oscillating Water Column Wave Energy Converter Device Using Representative Regular Waves of the Sea State Found in Tramandaí, Brazil. *Processes*, *12*(11). https://doi.org/10.3390/pr12112352

Nguyen, D. T., Chow, Y. C., & Lin, C. C. (2024). Modeling and performance estimation for L-shaped OWC wave energy converters with a theoretical correction for spring-like air compressibility. *Renewable Energy*, *237*. https://doi.org/10.1016/j.renene.2024.121499

Ning, D., Fu, L., Zhou, Y., Mayon, R., & Zhang, Y. (2024). Hydrodynamic performance of a land-based multi-chamber OWC wave energy capture system: An experimental study. *Coastal Engineering*, *190*. https://doi.org/10.1016/j.coastaleng.2024.104510

Ning, D., Wang, R., & Zhang, C. (2017). Numerical simulation of a dual-chamber oscillating water column wave energy converter. *Sustainability (Switzerland)*, *9*(9). https://doi.org/10.3390/su9091599

Ning, D. zhi, Wang, R. quan, Chen, L. fen, & Sun, K. (2019). Experimental investigation of a land-based dual-chamber OWC wave energy converter. *Renewable and Sustainable Energy Reviews*, *105*, 48–60. https://doi.org/10.1016/j.rser.2019.01.043

Palmer, H., Zhao, M., Wu, H., Hu, P., Mia, M. R., & Lei, C. (2023). Improved performance of land-fixed oscillating water column through dual chamber design. *Ocean Engineering*, *290*. https://doi.org/10.1016/j.oceaneng.2023.116389

Putri, D. L., Adnyani, L. P., Nurmawati, Wirawan, M. K., Kurniawati, D. M., Kharim, M., Haq, J. A. K., & Marta, A. S. D. (2026). Experimental Analysis of L-Shaped Oscillating Water Column with Horizontal Chamber Length Variations under Different Wave Periods. *Evergreen*, *13*(1), 200–211. https://doi.org/10.5109/7407645

Rezanejad, K., Gadelho, J. F. M., Xu, S., & Guedes Soares, C. (2021). Experimental investigation on the hydrodynamic performance of a new type floating Oscillating Water Column device with dual-chambers. *Ocean Engineering*, *234*. https://doi.org/10.1016/j.oceaneng.2021.109307

Rezanejad, K., Souto-Iglesias, A., & Guedes Soares, C. (2019). Experimental investigation on the hydrodynamic performance of an L-shaped duct oscillating water column wave energy converter. *Ocean Engineering*, *173*, 388–398. https://doi.org/10.1016/j.oceaneng.2019.01.009

Rodríguez, A. A. M., Ilzarbe, J. M. B., Casarín, R. S., & Ereño, U. I. (2020). The influence of the chamber configuration on the hydrodynamic efficiency of oscillating water column devices. *Journal of Marine Science and Engineering*, *8*(10), 1–27. https://doi.org/10.3390/jmse8100751

Samak, M. M., Elgamal, H., & Nagib Elmekawy, A. M. (2021). The contribution of L-shaped front wall in the improvement of the oscillating water column wave energy converter performance. *Energy*, *226*. https://doi.org/10.1016/j.energy.2021.120421

Schaffer, H. A. (n.d.). Pergamon SECOND-ORDER WAVEMAKER THEORY FOR IRREGULAR WAVES. In *Ocean Engng* (Vol. 23, Issue 1).

Supriyanto, E., Rohman, A. T., Malakani, A. I., Ikhsanudin, I. Y., Wibowo, A., Suryantoro, M. T., Musthofa, A., Soewono, R. T., Helios, M. P., Nugraha, A. D., Deendarlianto, & Marta, A. S. D. (2025). Experimental study of flow characteristics in hydrodynamic and aerodynamic L-shaped and U-shaped oscillating water column chambers. *Results in Engineering*, *25*. https://doi.org/10.1016/j.rineng.2024.103762

Tan, L., Chang, R., & Ikoma, T. (2024). Numerical analysis of a projecting wall type oscillating water column (PW-OWC) wave energy converter in regular waves. *Journal of Hydrodynamics*, *36*(3), 479–491. https://doi.org/10.1007/s42241-024-0041-7

Wang, C., Zhang, Y., & Deng, Z. (2022). A novel dual-chamber oscillating water column system with dual lip-wall pitching motions for wave energy conversion. *Energy*, *246*. https://doi.org/10.1016/j.energy.2022.123319

Wang, R. quan, Ning, D. zhi, & Zou, Q. ping. (2020). Wave loads on a land-based dual-chamber Oscillating Water Column wave energy device. *Coastal Engineering*, *160*. https://doi.org/10.1016/j.coastaleng.2020.103744

Zhao, X., Zhang, L., Li, M., & Johanning, L. (2021). Experimental investigation on the hydrodynamic performance of a multi-chamber OWC-breakwater. *Renewable and Sustainable Energy Reviews*, *150*. https://doi.org/10.1016/j.rser.2021.111512

Zheng, S., Antonini, A., Zhang, Y., Miles, J., Greaves, D., Zhu, G., & Iglesias, G. (2020). Hydrodynamic performance of a multi-Oscillating Water Column (OWC) platform. *Applied Ocean Research*, *99*. https://doi.org/10.1016/j.apor.2020.102168